The payne effect: primarily polymer-related or filler-related phenomenon?

Nadhatai Warasitthinon, Anne-Caroline Genix, Michael Sztucki, Julian Oberdisse, Christopher G. Robertson

The Payne Effect: Primarily Polymer-Related or Filler-Related Phenomenon?

Nadhatai Warasitthinon,[a] Anne-Caroline Genix,[b,*] Michael Sztucki,[c] Julian Oberdisse,[b] and Christopher G. Robertson[a,#,*]

[a] Cooper Tire & Rubber Company, 701 Lima Ave, Findlay, OH 45840, USA

[b] Laboratoire Charles Coulomb (L2C), University of Montpellier, CNRS, 34095 Montpellier, France

[c] European Synchrotron Radiation Facility, 71 Avenue des Martyrs, BP 220, F-38043, Grenoble Cedex 9, France

ABSTRACT

The hysteretic softening at small dynamic strains (Payne effect) – related to the rolling resistance and viscoelastic losses of tires – was studied as a function of particle size, filler volume fraction, and temperature for carbon black (CB) reinforced uncrosslinked styrene-butadiene rubber (SBR) and a paste-like material composed of CB-filled paraffin oil. The low strain limit for dynamic storage modulus was found to be remarkably similar for CB-filled oil compared to CB-filled SBR. Small-angle X-ray scattering (SAXS) measurements on the simple composites and detailed data analysis confirmed that the aggregate structures and nature of filler branching/networking of carbon black were virtually identical within oil compared to the high molecular weight polymer matrix. The combined dynamic rheology and SAXS results provide clear evidence that the deformation-induced breaking (unjamming) of the filler network – characterized by filler-filler contacts that are percolated throughout the material – is the main cause for the Payne effect. However, the polymer matrix does play a secondary role as demonstrated by a reduction in Payne effect magnitude with increasing temperature for the CB-reinforced rubber, which was not observed to a significant extent for the oil-CB system.

* Corresponding authors: cgrobertson@endurica.com; anne-caroline.genix@umontpellier.fr

[#] present address: Endurica LLC, 1219 West Main Cross St, Findlay, OH 45840, USA

INTRODUCTION

For amorphous polymers and their crosslinked networks at temperatures above the glass transition, the onset of strain-dependent (nonlinear) dynamic mechanical properties generally takes place at relatively high strains (> 50%). Once filler particles are introduced into these elastomeric materials at sufficient loading and polymer nanocomposites (PNCs) are formed, however, striking strain dependences of storage modulus (G') and loss modulus (G") occur at low oscillatory strain amplitudes (e.g., in the range from 0.1% to 10%). Dillon, Prettyman, and Hall [1] were the first to document such nonlinear behavior, followed by Fletcher and Gent.[2] It was Payne's influential paper [3] and subsequent contributions to the literature, however, which solidified this hysteretic softening behavior at low dynamic strains as a key viscoelastic signature of filled rubbers. Therefore, the phenomenon is generally called the Payne effect in both academic and industrial communities. We use this term because it is the most recognizable name for the behavior, but we acknowledge the earlier discoveries. The main characteristics of this dynamic mechanical behavior are covered in a book chapter by Klüppel and Heinrich [4] and in a brief review.[5]

The Kraus model [6] was the first mathematical approach offered to describe the Payne effect, and it is based on the breaking and reforming of the filler network. Another well-established model that derives predictions for the Payne effect from a different foundation involving polymer debonding from filler is the Maier-Göritz model. [7] These two models are both widely employed to fit strain-dependent dynamic storage and loss moduli of filled rubber, despite their very different fundamental origins.

The proposition by Kraus is based on the evolution of the filler network with strain, and it is therefore essential to quantitatively characterize the nanostructure of this network. The main methods used in the literature are either electron microscopy, and in particular transmission electron microscropy (TEM), and small-angle scattering of neutrons or X-rays (SANS and SAXS).[8-11] The key advantage of direct imaging techniques is the more straightforward analysis. Well-known drawbacks include the low statistical significance of a (very) small piece of sample in the field of vision, as well as problems to actually see particle structures and correlations in dense polymer nanocomposites – which are the ones of interest for applications. Cutting thin slices for observation in TEM is a possible way out, if many such samples can be observed. [12] Sometimes, quantitative analysis is possible based on some hypothesis on the extension of observed aggregates in the third dimension. [13] True three-dimensional observation by electron microscopy is much more involved, as proposed by Dalmas et al. [14-15] Small-angle scattering allows a statistically more relevant structural analysis, in particular due to averaging over macroscopic

quantities in the beam, at the expense of a more involved data analysis, which however gives access to correlations even in dense media. [16] The typical structure of highly loaded polymer nanocomposites is of multi-scale nature and can be subdivided in three parts: [17] (a) (polydisperse) primary particles, usually in the nano-range, (b) fused aggregates containing some tens of primary particles, and (c) a large-scale (LS) space-filling structure of branches containing the aggregates. In scattering, these different structural levels contribute in different q-ranges, and can thus be separated. Many of the multi-scale structures of silica or carbon black (CB) dispersed in polymer adopt a fractal structure, [18-20] and they are usually well-described by the Beaucage model. [21-22] If one goes a step further in the description of interactions, it is possible to extract not only characteristic sizes of nanoparticles (NPs) and aggregates but also virial coefficients of interaction potentials [23-24] and local densities.[25] In a comprehensive approach of multi-scale structure, we have proposed a coherent quantitative analysis of small-angle data based on the average NP radius, the number of particles in each aggregate, aggregate size and density, and the characteristic size of large scale branches filling the sample.[11, 26] Alternatively, if sufficient knowledge is available on the primary particles, e.g., if it is possible to measure them under dilute conditions in order to describe shape, polydispersity, and surface roughness quantitatively, then reverse Monte Carlo modelling may be used for a quantitative analysis of the particle and aggregate structure. [27-28] This technique provides a series of real space snapshots with particle distributions, which are compatible with the observed scattered intensity. In the present contribution on more or less ill-defined carbon black particles, the above-mentioned multi-scale approach had to be used. It is based on the extraction of robust features of the scattered intensities, like Guinier domains indicating characteristic sizes, breaks in slope or equivalently maxima in $q^n I(q)$ presentations as done below, power law exponents, or peak positions. It provides average values for any characteristic size (aggregates, particles), which is highly trustworthy due to the averaging over the entire sample in the beam.

One interesting and controversial aspect of the Payne effect is that the extent of the small strain reinforcement – quantified from the limiting value of G' below the onset of strain-induced softening (G'_0) – decreases with increasing temperature. The magnitude of the Payne effect diminishes as temperature is increased, and a representative example from the literature can be cited for silica-reinforced crosslinked poly(dimethyl siloxane) (PDMS).[29] The glass-transition temperature of PDMS is about -130 °C, yet the Payne effect persists at 80 °C, so it is difficult to rationalize polymer segmental dynamics (glass transition response) being solely responsible for the phenomenon,[30-31] although the polymer can still be immobilized near the particles surfaces in terms of longer-time chain dynamics.[32]

There are various mechanisms proposed in the literature to explain the thermal weakening of the Payne effect: (1) an effect from the filler network itself wherein filler-filler interactions reversibly dissociate with increasing temperature;[6, 33] (2) temperature-dependent slippage / desorption of polymer chains at the filler NP surfaces; [7, 34] (3) reduced thickness of an immobilized polymer layer around NPs (glassy shell) as temperature is increased; [35-38] and (4) thermal expansion of the polymer matrix with heating, which increases the distances between filler particles, thus lessening the interactions between particles. [39]

The question remains concerning whether the Payne effect is primarily due to the breaking of a percolated filler network or if it arises mainly from dynamics of polymer chains at the interface with the NPs. This present study attempts to resolve this by contrasting strain-dependent viscoelastic results for carbon black reinforced styrene-butadiene rubber (SBR) and CB-filled paraffin oil, with some results presented recently. [40] Two different NP sizes were used, a range of particle concentrations was studied, and the influence of temperature on the behavior was considered. The similar values of dynamic storage modulus in the low strain amplitude region (G'_0) for particle-filled low molecular weight liquid and filled rubber was demonstrated by Payne for carbon black filled oil versus butyl rubber, [41] and by Payne and Whittaker for water-clay pastes and clay-filled natural rubber. [42] For the comparison between CB in a polymer matrix and in oil to be valid, the filler structure in both matrices needs to be as close as possible, which had never been verified before. We have therefore analyzed the microstructure of four representative samples made of two CB grades in the two matrices using a combination of TEM and SAXS, accompanied by a state-of-the-art quantitative analysis as outlined above, and put them into perspective with the rheological results.

MATERIALS AND METHODS

Polymer, carbon black, and mineral oil: The solution styrene-butadiene rubber used was Asahi Tufdene 2100R, which has 25 wt.% styrene and with 11% of the butadiene polymerized in 1,2 (vinyl) configuration. This polymer microstructure yields a glass-transition temperature of -65 °C. The Mooney viscosity is 78 at 100 °C for this SBR. Two different grades of carbon black from Cabot Corporation were used: N234 and N550. The paraffin oil was Equate™ mineral oil.

Formulations: Four compositions were studied for each CB type with each matrix material. The mixtures with N234 CB were made using 35, 50, 65, and 80 parts by weight of CB relative to 100 parts of either SBR or paraffin oil. The levels of N550 CB used to reinforce SBR and paraffin oil were 50, 65, 80, and 95 parts, with the higher range studied due to lower surface area and less

reinforcing nature of N550 compared to N234. Values of filler volume fraction (ϕ) were calculated from the formulations using density values of 0.87, 0.93, and 1.8 g/cm^3 for the oil, SBR, and CB, respectively.

Mixing: The carbon black and oil pastes were mixed in 20 g batches at room temperature using a high-speed centrifugal mixer (SpeedMixer, DAC 150 FVZ) [43] with the following stepwise procedure: 1 minute at 800 rpm, 1 minute at 2200 rpm, and 3 minutes at 3100 rpm. Two batches were made for each CB-oil composition, and the two replicates were each split in half and cross combined through additional mixing for 1 minute at 3100 rpm. The compounds containing CB and SBR were formed by mixing with a C.W. Brabender Instruments Inc. Prep-Mixer series 350 internal mixer. Compounds were mixed for 5 minutes at 50 rpm using a starting chamber temperature of 90 °C. Note that the styrene-butadiene matrix has not been crosslinked.

Rheology: The viscoelastic properties of the oil-CB and SBR-CB mixtures were characterized in oscillatory shear using a MonTech D-RPA 3000 Dynamic Rubber Process Analyzer (RPA). Three temperatures of 30, 50, and 70 °C were used. After loading a sample in the RPA, a hold of 2 minutes without deformation was applied before starting a logarithmically-spaced strain amplitude sweep from 0.03% to 45%. The viscosity of the paraffin oil was measured at 25°C using a Model DV-II Pro Viscometer manufactured by Brookfield Engineering Labs Inc. Rotational speeds of 10, 20, 50, and 100 rpm were utilized with two different spindles (31 and 34), and the torque results were converted to viscosity data using known relationships for the testing geometries.

Structural analysis: Small-angle X-ray scattering was performed on beamline ID02 [44] at the European Synchrotron Radiation Facility (ESRF, Grenoble FR) at a wavelength λ = 1 Å using 3 configurations defined by a sample to detector distance D = 1 m, 10 m and 30 m, yielding a q-range from 2 10^{-4} to 0.7 Å^{-1}. The scattering of pure SBR and paraffin oil have been measured independently to subtract the matrix contribution, (1 - ϕ) I_{matrix}, to each filled sample. The carbon black particle morphologies were investigated at Birla Carbon by transmission electron microscopy using an FEI Tecnai F20 TEM operating at 200 kV. Carbon black dispersions on TEM grids were prepared according to the methodology of ASTM D3849 for dry carbon black samples.

RESULTS AND DISCUSSION

The paraffin oil and high molecular weight styrene-butadiene rubber are very different materials to consider as matrices in composites reinforced by carbon black. Shear viscosity results indicate a low viscosity of 0.15 Pa.s for the paraffin oil at 25 °C, and the viscosity is independent of shear rate (Newtonian), which means that the oil has zero dynamic storage

modulus. In contrast, the SBR has a dynamic viscosity (η^*) of 6900 Pa.s and a strain-independent storage modulus of 0.44 MPa from RPA testing at 30 °C and 10 Hz. The two carbon black grades that were incorporated into the oil-CB and SBR-CB mixtures have different particle size characteristics as summarized in Table 1, [45] with N234 having more reinforcing potential than N550. This corresponds to specific surface areas of 120 and 41 m²/g for N234 and N550, respectively.[45]

Table 1: Characteristics of CB in two matrices extracted from SAXS data

CB	Matrix	ϕ	R_{NP} (nm)[(a)] SAXS	R_{agg} (nm) [(a)] SAXS	R_{LS} (nm)[(a)] SAXS	R_{NP} (nm)[(b)] TEM	R_{agg} (nm) [(b)] TEM
N234	Oil	0.239	7.5	26	300	10.5 ± 4.5	33.0 ± 16
N234	SBR	0.251	7.1	25	250		
N550	Oil	0.239	17.0	73	480	26.5 ± 14	69.5 ± 35
N550	SBR	0.251	16.3	72	460		

[(a)] SAXS results for primary NP radius R_{NP}, aggregate radius R_{agg}, and large-scale characteristic lateral size R_{LS}, with the latter deduced from low-q break in slope;
[(b)] Literature values for R_{NP} and R_{agg} from transmission electron microscopy for nominally identical CB grades to those used in our study. [45]

Adding the CB particles to the paraffin oil transformed the free-flowing liquid into a paste with a jammed structure that does not creep under its own weight as illustrated in Figure 1. Note that the time evolution of such CB-loaded pastes has been studied by Jiang et al, [46] in combination with electron microscopy and SAXS. They provide evidence, in particular the observation of a low-q upturn, for filler network formation from disconnected aggregates with time close to the percolation threshold accompanied by an increase in elastic modulus and conductivity. For the present purpose, a macroscopic illustration as in Figure 1 of the jammed nature of the paste is sufficient.

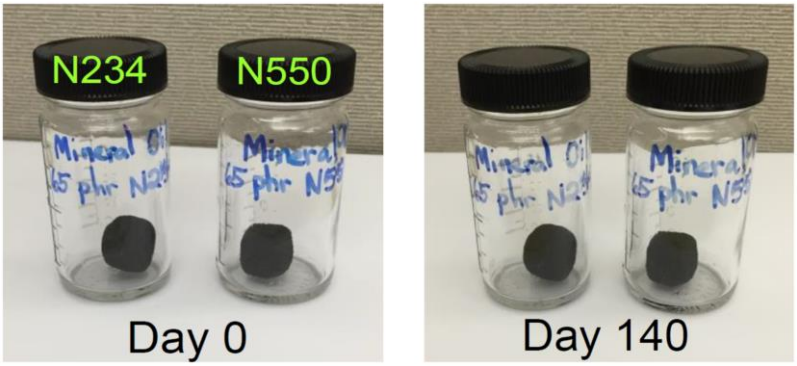

Figure 1. Photographs of CB-oil pastes (ϕ = 0.24) to illustrate absence of gravity-driven flow for the materials at room temperature.

The rheological response at larger strain, however, shows that the oil-material has a tendency to flow, in the sense that the loss modulus exceeds the storage modulus as a function of strain in oscillatory shear experiments, as exemplarily shown in Figure 2a for N234-filled oil. In polymer, the nanocomposite made with the same carbon black presents no indication of flow onset as seen in Figure 2b. The polymer thus contributes to the yield behavior of the material, presumably due to large-scale connectivity (entanglements, possibly immobilized polymer layers) mediated by long chains. On the other hand, we will see below that the low-strain behavior of both types of samples, oil- and polymer-based, is similar, and in particular the Payne effect exists for both matrices.

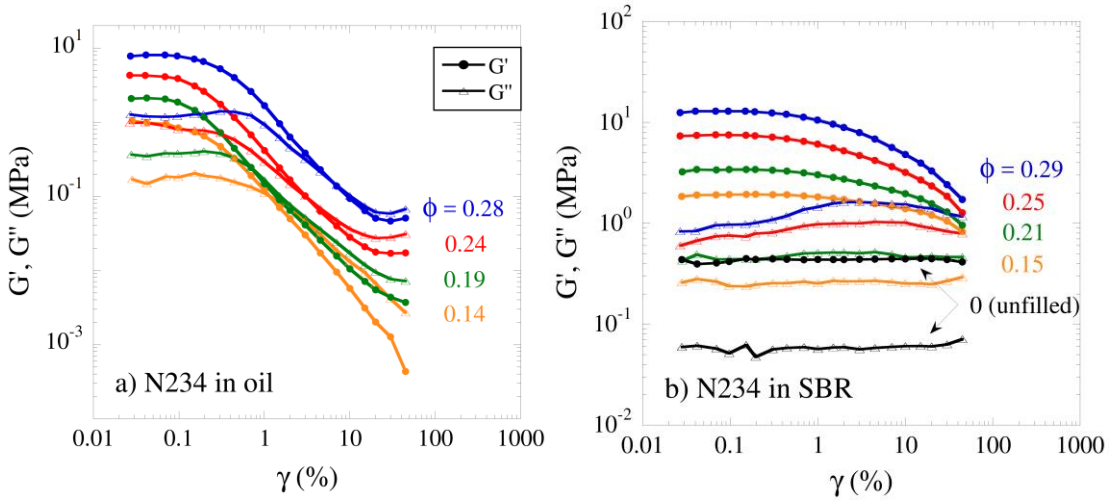

Figure 2. Storage and loss moduli versus strain amplitude at T = 30 °C and f = 10 Hz for N234-filled oil **(a)** and N234-filled SBR **(b)**. Note the different y-axis scaling in **a)** and **b)**.

Structural analysis of the filler on the nanoscale has been performed by SAXS and TEM. Transmission electron microscopy pictures of the filler NPs have been obtained to characterize the structure of the primary particles and fused aggregates under dilute conditions. In Figure 3, representative TEM images for the two carbon black grades are shown. The different nanoparticle size is clearly visible, with high polydispersity, for N234 and N550. Their typical size is compatible with the data provided in the literature for these grades (Table 1). On larger scales, these NPs are organized in ill-defined structures as shown in the micrographs (a few hundred nm). The latter are concentrated in the final nanocomposites. As we will see below, an intermediate structural level is also present, corresponding to an aggregate containing several tens of primary NPs as illustrated in the right picture.

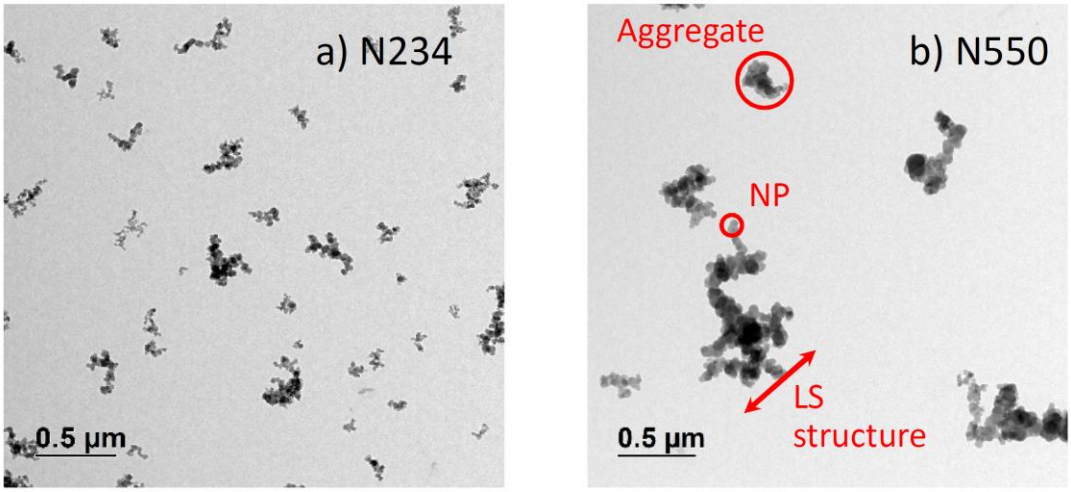

Figure 3. TEM pictures of **(a)** N234 and **(b)** N550 carbon black primary particles and aggregates obtained by sonication. Scale bar = 0.5 µm. The arrow illustrates structure formation on a larger scale.

SAXS experiments allow characterizing the filler and filler network structure within highly loaded PNCs. Scattering measurements have been performed with the four samples containing either N234 or N550, in paraffin oil or in styrene-butadiene rubber. The results in absolute units are shown in Figure 4a. There is a remarkable agreement in shape between all curves above q = 0.01 $Å^{-1}$, with a slight vertical shift indicating that the N550 nanoparticles are bigger than the N234 ones. A quantitative analysis is proposed below. There is even perfect pair-wise superposition above 0.2 $Å^{-1}$, suggesting that the local atomic structure and in particular surface roughness of the primary CB particles is the same for both N234 and N550. The differences in the low- to intermediate-q range, between 0.001 and 0.01 $Å^{-1}$, indicate different aggregate structure, i.e. in the 100-nm range, for both CBs.

The next observation in Figure 4a is that there are two families of curves, associated with the two matrices. In spite of the close filler volume fractions (ca. 0.24 – 0.25) of all samples, the samples with a mineral oil matrix display higher intensities. This is caused by the higher X-ray contrast of the CB nanoparticles in oil, which is a general prefactor of the scattered intensity, just like the volume fraction. One can highlight the structural features by renormalizing the contrast of the scattered intensity in oil to the one in SBR. The result of this renormalization is shown in Figure 4b. The good superposition of the two curves for each carbon black demonstrates that the general structure of the CBs is independent of the matrix type. Without any quantitative analysis or modeling, one of the main conclusions of this article is thus that the CBs adopt very similar structures on the nanoscale in oil and SBR.

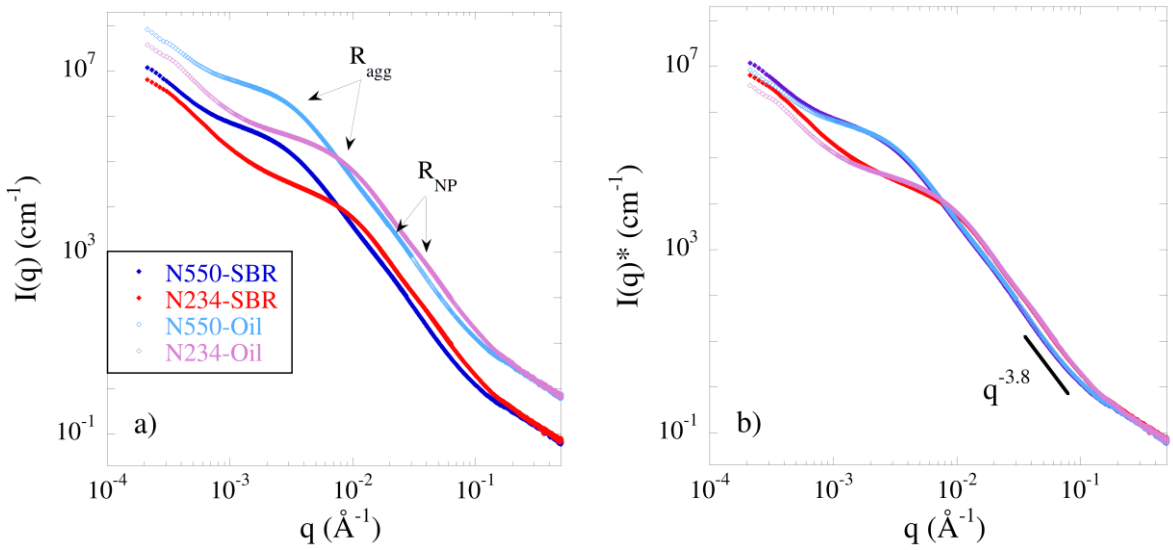

Figure 4: SAXS intensities as a function of wave vector q for N234 and N550 CB in oil or SBR. **a)** Absolute units (cm^{-1}). **b)** Intensities of oil-samples renormalized to corresponding SBR-nanocomposites.

The structure of each CB in either oil or SBR can be analyzed quantitatively. In Figure 4b, the high-q scattering follows a power law ($q^{-3.8}$) which is related to the (identical) surface roughness, presumably of fractal nature with surface fractal dimension of 2.2, of the CB [19]. Careful data treatment of the scattering in this q-range and proposed below reveals the typical size of the primary particle. Around 0.01 $Å^{-1}$, the intensity then levels off, and the position in q of this break in slope is characteristic of the typical aggregate size. Moreover, the intensity level in this zone can be used to extract the local density of aggregates using a correlation hole analysis developed by some of us. [11, 25] The fact that the curves superimpose for both matrices show again that also these local aggregate densities are independent of the matrix type. At low q, finally, the intensities increase strongly, which is reminiscent of a large-scale filler organization. This result is interesting because it is often difficult to attribute the low-q upturn in scattering to filler structure, as crazes or bubbles in polymer may result in a similar signature, compromising the observation. Here such a signal pollution can be ruled out unambiguously, because the same scattering is observed in oil, where such phenomena do not exist. The break in slope observed around 0.001 $Å^{-1}$ is thus a measure of a large-scale structure ($\propto \pi/q$), presumably the typical lateral size of branches which we term R_{LS}. We have determined the characteristic sizes with care reporting the corresponding values in Table 1. Focusing on the aggregate radius, R_{agg}, measurable around 0.01 $Å^{-1}$, we have plotted the data in a so-called Kratky presentation, i.e., $q^2I(q)$ vs q, as shown in Figure 5.

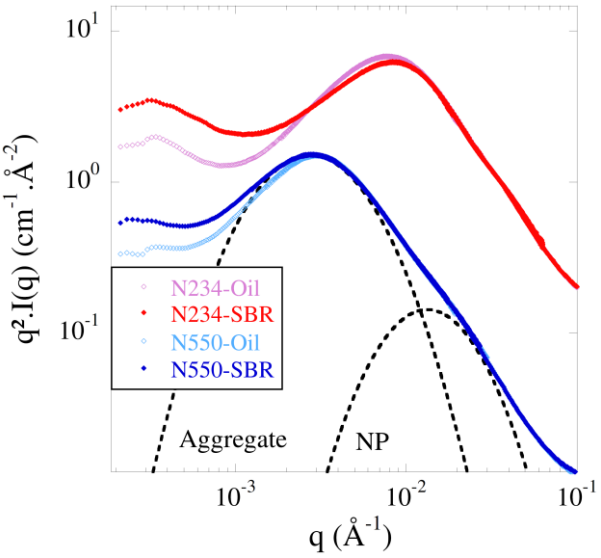

Figure 5: Kratky representation of the scattered intensities shown in Figure 4a. Data for N550 in oil and N234 in SBR have been shifted to match their counterpart (N550 in SBR and N234 in oil, respectively) at high q in order to superimpose scattering of same NPs. An example of fit using the sum of two log-normal functions is shown for N550-SBR.

The break in slope at intermediate q now becomes a well-identified maximum. The position of this maximum can be used to estimate the average radius of the aggregates, R_{agg}. Moreover, an additional shoulder at higher q is characteristic of the radius R_{NP} of the (polydisperse) primary particles. The superposition of the scattering over a large q range ($q > 2.10^{-3}$ Å^{-1}) in Figure 5, for a common filler dispersed in different matrices demonstrates that filler structure is not affected by the matrix. Both features, NPs and aggregates, can be quantitatively described using the sum of two log-normal functions [11] as superimposed in Figure 5. This procedure allows determining both R_{agg} (deduced from the log-normal position parameter, $R_{agg} = \pi/q_0$) and R_{NP} simultaneously. All results are summarized in Table 1.

Several conclusions can be drawn from the data in Table 1. First of all, our measurements of the NP and aggregate characteristics of the CBs correspond to classic literature values for N234 and N550. [45] Moreover, they agree with the typical sizes observed by TEM, cf. Figure 3. Secondly, the multi-scale structure of the filler stretches from primary NPs of typically 10 – 20 nm (depending on the CB grade65), to aggregates containing probably about twenty NPs and measuring typically four to five NP sizes in linear dimension. These aggregates form a large-scale network of characteristic length scale 250 to 500 nm. In both cases, the particle and aggregate radii of a same carbon black, as well as the local aggregate density, coincide closely,

independently of the matrix. This result confirms the abovementioned model-free conclusion of virtually identical structures in both paraffin oil and SBR.

We have shown in Figure 1 that the samples do not flow under gravity over periods of months. However, the application of increasing dynamic strain caused the oil-CB materials to progressively yield, giving Payne effect responses that are similar to CB-filled SBR behavior. For the CB grade N234, the corresponding measurements plotted on the same scales are presented in Figures 6a and 6b for CB in polymer and in oil, respectively. Equivalent results for N550 are reported in Figures 7a and 7b.

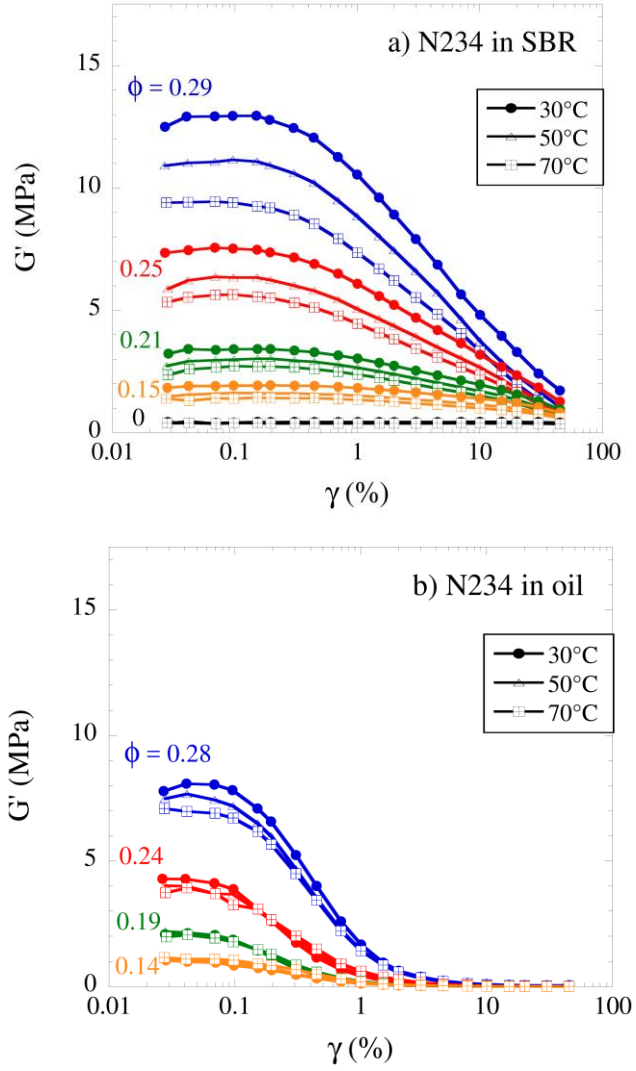

Figure 6. Strain dependent G' (Payne effect) at f = 10 Hz and different temperatures (T = 30, 50 and 70°C) for N234-filled SBR **(a)** and N234-filled oil **(b)**. Black symbols in **a)** represent the unfilled SBR matrix.

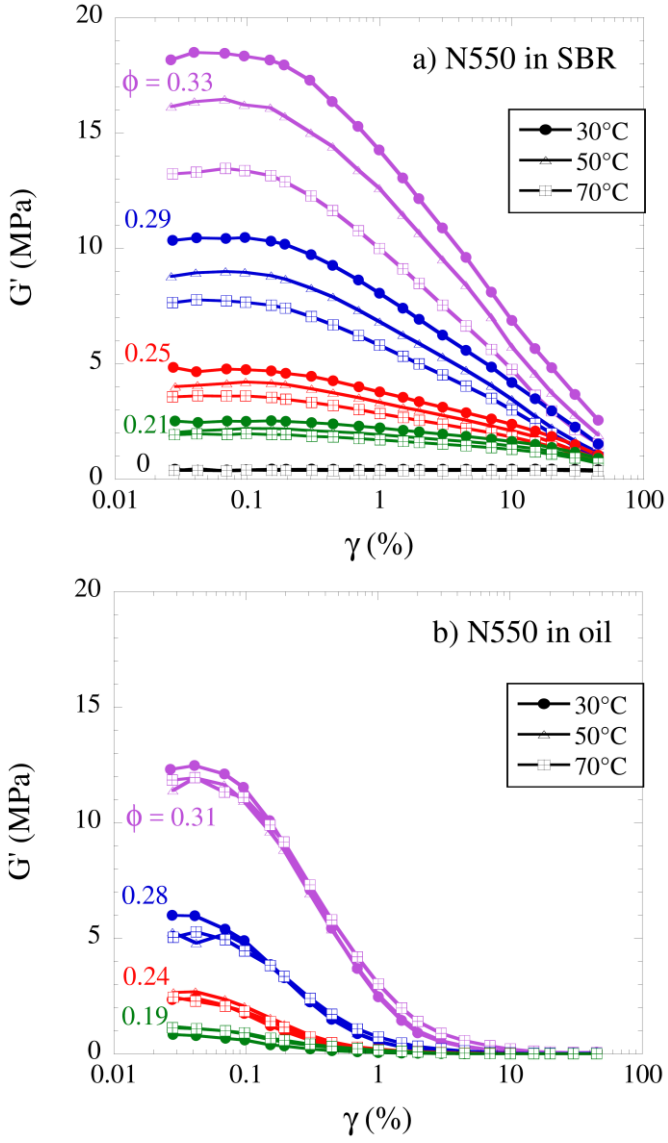

Figure 7. Strain dependent G' (Payne effect) at f = 10 Hz and different temperatures (T = 30, 50 and 70°C) for N550-filled SBR **(a)** and N550-filled oil **(b)**. Black symbols in **a)** represent the unfilled SBR matrix.

In Figures 6 and 7, the evolution of the storage modulus is found to depend on the three experimental parameters: strain, temperature, and filler content. As a function of strain in polymer nanocomposites in Figure 6a (resp. 7a), the well-known softening of the modulus is found, evidencing the Payne effect. One may note that a general statistical mechanics approach mapping the jamming/unjamming transition on an Ising model has been proposed to explain the softening, [47] leading to a universal power law prediction as observed in the literature. Our results also display an onset of a high-deformation power law, but it does not give access to a well-defined exponent. For the sake of completeness, it is mentioned that other theoretical approaches

based on statistical network properties described by a high number of parameters exist. [48-49] In the oil-based materials of Figure 6b (resp. 7b), the Payne effect is also observed, with a well-established high-deformation power law of exponent between 0.5 and 1, compatible with model predictions.[4, 47] A characteristic weakening of the Payne effect in polymer nanocomposites with increasing temperature is measured in Figures 6a and 7a, whereas in the oil-CB materials, no thermal softening was found in Figures 6b and 7b, except possibly for a minor effect at the highest particle loading (ϕ = 0.28 – 0.31). Therefore, the polymer matrix appears to play a secondary role in the Payne effect, with the predominant contribution coming from the filler network, and a temperature-dependent part induced by the polymer. In the present case, the comparatively minor polymer contribution is related to interfacial chain conformations and their dynamics and relaxation. Also, we have shown in Figure 2 that the polymer matrix impedes extensive strain softening that is observed with CB-filled oil. Structurally, it is probable that the stress-carrying filler network breaks under strain, and in oil there are no restoring forces capable of maintaining elasticity, a role the polymer can play. The difference in flow observed in Figure 2 may thus be connected to the difference in the higher strain region in Figures 6 and 7: the storage modulus of the oil-CB pastes dropped to very small values (G' < 0.1 MPa), a phenomenon which is not present with the SBR matrix in the same Figure. One may note that the unfilled SBR had G' > G" due to substantial entanglement contributions that were not relaxed at the frequency and temperatures studied, which explains the viscoelastic differences between oil-CB and SBR-CB in the higher dynamic strain region. In conclusion, the comparison of Figures 6a and 6b, resp.7a and 7b, demonstrates the strong similarity in the (low strain) Payne effect between CB-oil materials, and polymer nanocomposites containing the same filler.

Finally, as a function of filler content, the reinforcement effect of increasing modulus with ϕ is observed in Figures 6a and 6b for N234, and in Figures 7a and 7b for N550. Moreover, the dependence of the Payne effect on the filler content is easily seen. The order of magnitude of the limiting (strain-independent) values of G' in the low dynamic strain region, $G'_0 = G'(\gamma \rightarrow 0)$, is similar for oil-CB relative to SBR-CB materials when compared at similar carbon black volume fractions, which gives strong support for the idea that stiffness in this region was produced almost exclusively by the network of percolated filler-filler contacts throughout the composites. The low strain G'_0 versus ϕ plots in Figure 8 show the influence of the CB particles on the storage modulus at temperatures of 30 °C and 70 °C.

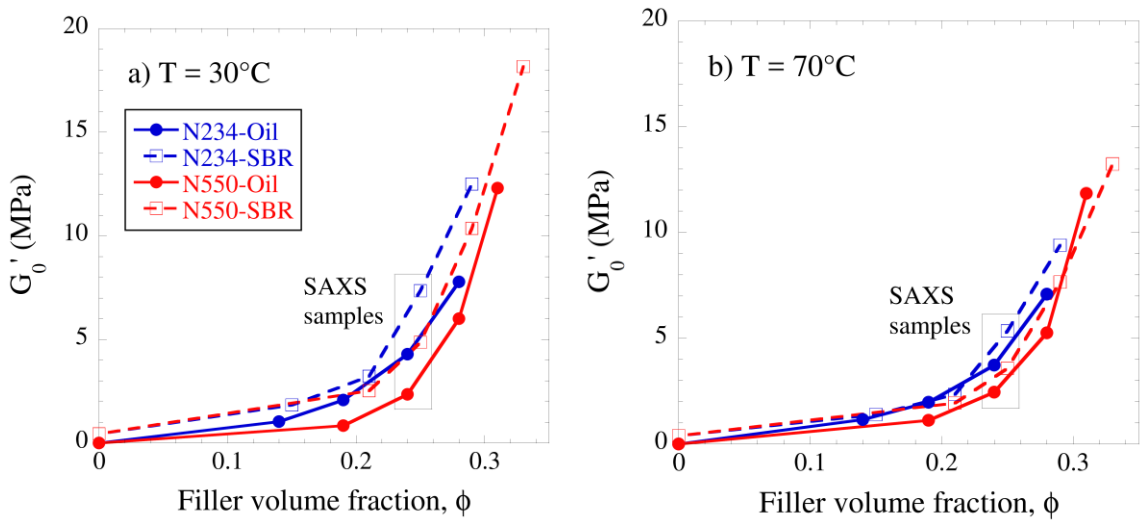

Figure 8. G'_0 versus ϕ (f = 10 Hz, γ = 0.03%) for CB-filled paraffin oil (solid symbols) and CB-filled SBR (empty symbols) at T = 30 °C **(a)** and 70 °C **(b)**.

The low-strain modulus in Figure 8 displays a standard evolution with filler content: first a moderate increase due to hydrodynamic interactions [50-51] and followed by a strong upturn due to percolation of the filler network. At 70 °C, the G'_0 values are essentially the same for the oil and SBR systems throughout the whole range of ϕ when reinforced by the same type of carbon black, whereas the polymer matrix composites have moderately higher G'_0 at the lower temperature of 30 °C. This illustrates again that there is a temperature-dependent contribution of the polymer to the Payne effect, while the main part of the mechanical response as illustrated by the general shape of the curve in Figure 8 is caused by the filler network. The temperature-induced weakening of the polymeric contribution in the CB-filled materials combined with the absence of weakening in oil results in a better agreement of the moduli at high temperature. It should be recalled that the G' for the unfilled SBR is 0.44 MPa while the G' for the neat paraffin oil is 0 MPa, which is why the additional contribution of the filler network dominates the low-strain filler reinforcement, and a similar behavior is observed with the polymer matrix. This is related to the virtually identical particle network structure, which is probably caused by particle-particle interactions outweighing the weak particle-matrix interactions in both cases. Indeed, the rubber does not possess attractive interactions with the NP interface, just like the mineral oil, and our results can thus probably be generalized to non-interacting rubber systems. On the contrary, strong interactions including matrices grafted to the NPs will necessitate further studies.

CONCLUSIONS

This study demonstrated that the Payne effect is primarily a filler-related phenomenon in carbon black filled polymer nanocomposites. The reinforcement of a low-viscosity paraffin oil by carbon black – to give a low-strain dynamic storage modulus that is similar to the value for a high molecular weight elastomer filled with the same amount of filler – can be explained by the additional presence of a load-supporting, three-dimensional network of filler-filler contacts. Small-angle X-ray scattering measurements on the composites demonstrated that the aggregate structures and nature of filler branching/networking of carbon black are virtually identical within oil compared to the rubber matrix. These filler networks within SBR and paraffin oil are sensitive to oscillatory strain amplitude, thus exhibiting the well-known Payne effect, which for a particle-filled viscous liquid involves a transition to flow behavior at higher dynamic strains. As a secondary influence, the presence of polymer chains introduces a thermal weakening of the filler network strength, with fundamental origin possibly due to softening and depercolation of immobilized polymer layers, [35-37] while the Payne effect is not significantly impacted by temperature when the matrix is paraffin oil. To conclude, a dominant part of the Payne effect is thus present regardless of the nature of the matrix – oil or polymer. The similarities in both filler structure and Payne effect of oil- and polymer-based materials – particularly visible at high temperature – suggest that filler structural rearrangements are the main cause of the Payne effect. Our observations are in line with others reported in the literature, [8] where it was concluded for a different system with polymer grafted NPs that breaking the filler network contributes more to the reinforcement effect than the matrix polymer, suggesting that our conclusion may be generalized to other polymer-particle systems.

There are significant research efforts underway at tire companies and raw materials suppliers to develop new materials and mixing approaches to reduce the magnitude of the Payne effect of rubber compounds for the next generation of improved fuel economy tires. It is hoped that the present clarification concerning the main filler networking origin of this strain-dependent viscoelastic behavior will help guide materials development in this field.

Acknowledgements: A.-C.G. and J.O. are thankful for support by the ANR NANODYN project, Grant ANR-14-CE22-0001-01 of the French Agence Nationale de la Recherche. The Center for High-rate Nanomanufacturing at UMass – Lowell is recognized for allowing the use of the high-speed mixer. Dr. Lewis Tunnicliffe and Dr. Ye Cai at Birla Carbon are acknowledged for providing

the TEM characterization of the CB particles. N.W. and C.G.R. are grateful to Cooper Tire & Rubber Company for approving this publication. The views presented are those of the collaborative research team and not those of any one individual or organization.

REFERENCES

(1) Dillon, J. H.; Prettyman, I. B.; Hall, G. L., Hysteretic and Elastic Properties of Rubberlike Materials under Dynamic Shear Stresses. *Journal of Applied Physics* **1944,** *15* (4), 309-323.

(2) Fletcher, W. P.; Gent, A. N., Nonlinearity in the Dynamic Properties of Vulcanized Rubber Compounds. *Rubber Chemistry and Technology* **1954,** *27* (1), 209-222.

(3) Payne, A. R., The Dynamic Properties of Carbon Black-Loaded Natural Rubber Vulcanizates. Part I. *J. Appl. Polym. Sci.* **1962,** *6* (19), 57-63.

(4) Heinrich, G.; Kluppel, M., Recent Advances in the Theory of Filler Networking in Elastomers. *Filled Elastomers Drug Delivery Systems* **2002,** *160*, 1-44.

(5) Robertson, C. G., Dynamic Mechanical Properties. In *Encyclopedia of Polymeric Nanomaterials*, Kobayashi, S.; Müllen, K., Eds. Springer Berlin Heidelberg: Berlin, Heidelberg, 2015; pp 647-654.

(6) Kraus, G., Mechanical Losses in Carbon-Black-Filled Rubbers. *Applied Polymer Symposia* **1984,** (39), 75-92.

(7) Maier, P. G.; Goritz, D., Molecular Interpretation of the Payne Effect. *Kautschuk Gummi Kunststoffe* **1996,** *49* (1), 18-21.

(8) Akcora, P.; Kumar, S. K.; Moll, J.; Lewis, S.; Schadler, L. S.; Li, Y.; Benicewicz, B. C.; Sandy, A.; Narayanan, S.; Illavsky, J.; Thiyagarajan, P.; Colby, R. H.; Douglas, J. F., "Gel-Like" Mechanical Reinforcement in Polymer Nanocomposite Melts. *Macromolecules* **2010,** *43* (2), 1003-1010.

(9) Janes, D. W.; Moll, J. F.; Harton, S. E.; Durning, C. J., Dispersion Morphology of Poly(Methyl Acrylate)/Silica Nanocomposites. *Macromolecules* **2011,** *44* (12), 4920-4927.

(10) Jouault, N.; Vallat, P.; Dalmas, F.; Said, S.; Jestin, J.; Boue, F., Well-Dispersed Fractal Aggregates as Filler in Polymer-Silica Nanocomposites: Long-Range Effects in Rheology. *Macromolecules* **2009,** *42* (6), 2031-2040.

(11) Baeza, G. P.; Genix, A. C.; Degrandcourt, C.; Petitjean, L.; Gummel, J.; Couty, M.; Oberdisse, J., Multiscale Filler Structure in Simplified Industrial Nanocomposite Silica/Sbr Systems Studied by Saxs and Tem. *Macromolecules* **2013,** *46* (1), 317-329.

(12) Bouaziz, A.; Jaziri, M.; Dalmas, F.; Massardier, V., Nanocomposites of Silica Reinforced Polypropylene: Correlation between Morphology and Properties. *Polymer Engineering & Science* **2014,** *54* (9), 2187-2196.

(13) Banc, A.; Genix, A. C.; Chirat, M.; Dupas, C.; Caillol, S.; Sztucki, M.; Oberdisse, J., Tuning Structure and Rheology of Silica-Latex Nanocomposites with the Molecular Weight of Matrix Chains: A Coupled Saxs-Tem-Simulation Approach. *Macromolecules* **2014,** *47* (9), 3219–3230.

(14) Dalmas, F.; Genevaz, N.; Roth, M.; Jestin, J.; Leroy, E., 3d Dispersion of Spherical Silica Nanoparticles in Polymer Nanocomposites: A Quantitative Study by Electron Tomography. *Macromolecules* **2014,** *47* (6), 2044-2051.

(15) Koneti, S.; Roiban, L.; Dalmas, F.; Langlois, C.; Gay, A.-S.; Cabiac, A.; Grenier, T.; Banjak, H.; Maxim, V.; Epicier, T., Fast Electron Tomography: Applications to Beam Sensitive Samples and in Situ Tem or Operando Environmental Tem Studies. *Materials Characterization* **2019,** *151*, 480-495.

(16) Genix, A.-C.; Oberdisse, J., Structure and Dynamics of Polymer Nanocomposites Studied by X-Ray and Neutron Scattering Techniques. *Current Opinion in Colloid & Interface Science* **2015,** *20* (4), 293-303.

(17) Shinohara, Y.; Kishimoto, H.; Yagi, N.; Amemiya, Y., Microscopic Observation of Aging of Silica Particles in Unvulcanized Rubber. *Macromolecules* **2010,** *43* (22), 9480-9487.

(18) Schaefer, D. W.; Rieker, T.; Agamalian, M.; Lin, J. S.; Fischer, D.; Sukumaran, S.; Chen, C. Y.; Beaucage, G.; Herd, C.; Ivie, J., Multilevel Structure of Reinforcing Silica and Carbon. *Journal of Applied Crystallography* **2000,** *33* (1), 587-591.

(19) Rieker, T. P.; Hindermann-Bischoff, M.; Ehrburger-Dolle, F., Small-Angle X-Ray Scattering Study of the Morphology of Carbon Black Mass Fractal Aggregates in Polymeric Composites. *Langmuir* **2000,** *16* (13), 5588-5592.

(20) Mihara, S.; Datta, R. N.; Dierkes, W. K.; Noordermeer, J. W. M.; Amino, N.; Ishikawa, Y.; Nishitsuji, S.; Takenaka, M., Ultra Small-Angle X-Ray Scattering Study of Flocculation in Silica-Filled Rubber. *Rubber Chemistry and Technology* **2014,** *87* (2), 348-359.

(21) Beaucage, G., Approximations Leading to a Unified Exponential/Power-Law Approach to Small-Angle Scattering. *J. Appl. Cryst.* **1995,** *28*, 717-728.

(22) Beaucage, G.; Ulibarri, T. A.; Black, E. P.; Schaefer, D. W., Multiple Size Scale Structures in Silica-Siloxane Composites Studied by Small-Angle Scattering. *Hybrid Organic-Inorganic Composites* **1995,** *585*, 97-111.

(23) Jin, Y.; Beaucage, G.; Vogtt, K.; Jiang, H.; Kuppa, V.; Kim, J.; Ilavsky, J.; Rackaitis, M.; Mulderig, A.; Rishi, K.; Narayanan, V., A Pseudo-Thermodynamic Description of Dispersion for Nanocomposites. *Polymer* **2017,** *129*, 32-43.

(24) Mulderig, A.; Beaucage, G.; Vogtt, K.; Jiang, H.; Jin, Y.; Clapp, L.; Henderson, D. C., Structural Emergence in Particle Dispersions. *Langmuir* **2017,** *33* (49), 14029-14037.

(25) Genix, A.-C.; Oberdisse, J., Determination of the Local Density of Polydisperse Nanoparticle Assemblies. *Soft Matter* **2017,** *13* (44), 8144-8155.

(26) Baeza, G. P.; Genix, A. C.; Degrandcourt, C.; Petitjean, L.; Gummel, J.; Schweins, R.; Couty, M.; Oberdisse, J., Effect of Grafting on Rheology and Structure of a Simplified Industrial Nanocomposite Silica/Sbr. *Macromolecules* **2013,** *46* (16), 6388–6394.

(27) Musino, D.; Genix, A.-C.; Chaussée, T.; Guy, L.; Meissner, N.; Kozak, R.; Bizien, T.; Oberdisse, J., Aggregate Formation of Surface-Modified Nanoparticles in Solvents and Polymer Nanocomposites. *Langmuir* **2018,** *34* (9), 3010-3020.

(28) Oberdisse, J.; Hine, P.; Pyckhout-Hintzen, W., Structure of Interacting Aggregates of Silica Particles for Elastomer Reinforcement. *Soft Matter* **2007,** *2*, 476-485.

(29) Clément, F.; Bokobza, L.; Monnerie, L., Investigation of the Payne Effect and Its Temperature Dependence on Silica-Filled Polydimethylsiloxane Networks. Part I: Experimental Results. *Rubber Chemistry and Technology* **2005,** *78* (2), 211-231.

(30) Huang, M.; Tunnicliffe, L. B.; Thomas, A. G.; Busfield, J. J. C., The Glass Transition, Segmental Relaxations and Viscoelastic Behaviour of Particulate-Reinforced Natural Rubber. *European Polymer Journal* **2015,** *67*, 232-241.

(31) Robertson, C. G.; Roland, C. M., Glass Transition and Interfacial Segmental Dynamics in Polymer-Particle Composites. *Rubber Chem. Technol.* **2008,** *81* (3), 506-522.

(32) Robertson, C. G.; Rackaitis, M., Further Consideration of Viscoelastic Two Glass Transition Behavior of Nanoparticle-Filled Polymers. *Macromolecules* **2011,** *44* (5), 1177-1181.

(33) Arai, K.; Ferry, J. D., Temperature-Dependence of Viscoelastic Properties of Carbon-Black-Filled Rubbers in Small Shearing Deformations. *Rubber Chemistry and Technology* **1986,** *59* (4), 592-604.

(34) Sternstein, S. S.; Amanuel, S.; Shofner, M. L., Reinforcement Mechanisms in Nanofilled Polymer Melts and Elastomers. *Rubber Chemistry and Technology* **2010,** *83* (2), 181-198.

(35) Mujtaba, A.; Keller, M.; Ilisch, S.; Radusch, H. J.; Beiner, M.; Thurn-Albrecht, T.; Saalwächter, K., Detection of Surface-Immobilized Components and Their Role in

Viscoelastic Reinforcement of Rubber–Silica Nanocomposites. *ACS Macro Letters* **2014,** *3* (5), 481-485.

(36) Long, D.; Lequeux, F., Heterogeneous Dynamics at the Glass Transition in Van Der Waals Liquids, in the Bulk and in Thin Films. *European Physical Journal E* **2001,** *4* (3), 371-387.

(37) Berriot, J.; Lequeux, F.; Monnerie, L.; Montes, H.; Long, D.; Sotta, P., Filler-Elastomer Interaction in Model Filled Rubbers, a H-1 Nmr Study. *Journal of Non-Crystalline Solids* **2002,** *307*, 719-724.

(38) Merabia, S.; Sotta, P.; Long, D. R., A Microscopic Model for the Reinforcement and the Nonlinear Behavior of Filled Elastomers and Thermoplastic Elastomers (Payne and Mullins Effects). *Macromolecules* **2008,** *41* (21), 8252-8266.

(39) Wang, X. R.; Robertson, C. G., Strain-Induced Nonlinearity of Filled Rubbers. *Physical Review E* **2005,** *72* (3).

(40) Warasitthinon, N.; Robertson, C. G., The Payne Effect: Primarily Polymer-Related or Filler-Related Phenomenon? . *Paper Presented at the Fall 194th Technical Meeting of the Rubber Division, ACS* **2018**, B20.

(41) Payne, A. R., Study of Carbon Black Structures in Rubber. *Rubber Chemistry and Technology* **1965,** *38* (2), 387-399.

(42) Payne, A. R.; Whittaker, R. E., Dynamic Properties of Materials. *Rheologica Acta* **1970,** *9* (1), 97-102.

(43) Fang, L.; Wei, M.; Warasitthinon, N.; Shen, J.; Jian, R.; Schmidt, D.; Barry, C.; Mead, J., Preparation and Properties of Styrene-Butadiene Rubber/Clay Nano Composites by Using Liquid Rubber/Clay Master Batches. *Rubber Chemistry and Technology* **2013,** *86* (1), 96-108.

(44) Narayanan, T.; Sztucki, M.; Van Vaerenbergh, P.; Leonardon, J.; Gorini, J.; Claustre, L.; Sever, F.; Morse, J.; Boesecke, P., A Multipurpose Instrument for Time-Resolved Ultra-Small-Angle and Coherent X-Ray Scattering. *Journal of Applied Crystallography* **2018,** *51* (6), 1511-1524.

(45) Hess, W. M.; McDonald, G. C., Improved Particle-Size Measurements on Pigments for Rubber. *Rubber Chemistry and Technology* **1983,** *56* (5), 892-917.

(46) Jiang, J.-S.; Guo, R.-H.; Chiu, Y.-S.; Hua, C.-C., Percolation Behaviors of Model Carbon Black Pastes. *Soft Matter* **2018,** *14* (48), 9786-9797.

(47) Heinrich, G.; Vilgis, T. A., A Statistical Mechanical Approach to the Payne Effect in Filled Rubbers. *Express Polymer Letters* **2015,** *9* (3), 291-299.

(48) Hentschke, R., The Payne Effect Revisited. *Express Polymer Letters* **2017,** *11* (4), 278–292.

(49) Hentschke, R., Macroscopic Mechanical Properties of Elastomer Nano-Composites Via Molecular and Analytical Modelling. *Soft Materials* **2018,** *16* (4), 315-326.

(50) Smallwood, H. M., Limiting Law of the Reinforcement of Rubber. *J Appl Phys* **1944,** *15*, 758-766.

(51) Guth, E., Theory of Filler Reinforcement. *Journal of Applied Physics* **1945,** *16*, 20-25.